Spectroscopic and Kinetic Studies of PKU−Inducing Mutants of Phenylalanine Hydroxylase: Arg158Gln and Glu280Lys

ARTICLE *in* JOURNAL OF THE AMERICAN CHEMICAL SOCIETY · JUNE 2003

Impact Factor: 12.11 · DOI: 10.1021/ja029106f · Source: PubMed

9 AUTHORS, INCLUDING:

Erik Wasinger
California State University, Chico
38 PUBLICATIONS **973** CITATIONS
SEE PROFILE

Supratim Datta
Indian Institute of Science Education and Re…
17 PUBLICATIONS **418** CITATIONS
SEE PROFILE

Natasa Mitić
National University of Ireland, Maynooth
29 PUBLICATIONS **849** CITATIONS
SEE PROFILE

Tara Acharya
PepsiCo Inc.
17 PUBLICATIONS **1,106** CITATIONS
SEE PROFILE

J|A|C|S
ARTICLES
Published on Web 04/19/2003

Spectroscopic and Kinetic Studies of PKU−Inducing Mutants of Phenylalanine Hydroxylase: Arg158Gln and Glu280Lys

Jyllian N. Kemsley,[†] Erik C. Wasinger,[†] Supratim Datta,[§] Nataša Mitić,[||] Tara Acharya,[||] Britt Hedman,[*,‡] John P. Caradonna,[*,§] Keith O. Hodgson,[*,†,‡] and Edward I. Solomon[*,†]

Department of Chemistry, Stanford University, Stanford, California 94305, Department of Chemistry, Boston University, Boston, Massachusetts 02215, Department of Chemistry, Yale University, New Haven, Connecticut 06520, and Stanford Synchrotron Radiation Laboratory, SLAC, Stanford University, Stanford, California 94309

Received October 25, 2002; E-mail: edward.solomon@stanford.edu; hodgson@ssrl.slac.stanford.edu; caradonn@bu.edu; hedman@ssrl.slac.stanford.edu

Abstract: Phenylalanine hydroxylase (PAH) is a tetrahydrobiopterin-dependent, nonheme iron enzyme that catalyzes the hydroxylation of L-Phe to L-Tyr in the rate-limiting step of phenylalanine catabolism. This reaction is tightly coupled in the wild-type enzyme to oxidation of the tetrahydropterin cofactor. Dysfunction of PAH activity in humans leads to the disease phenylketonuria (PKU). We have investigated two PKU-inducing mutants, Arg158Gln and Glu280Lys, using kinetic methods, magnetic circular dichrosim (MCD) spectroscopy, and X-ray absorption spectroscopy (XAS). Analysis of the products produced by the mutant enzymes shows that although both oxidize pterin at more than twice the rate of wild-type enzyme, these reactions are only ~20% coupled to production of L-Tyr. Previous MCD and XAS studies had demonstrated that the resting Fe^{II} site is six-coordinate in the wild-type enzyme and converts to a five-coordinate site when both L-Phe and reduced pterin are present in the active site. Although the Arg158Gln mutant forms the five-coordinate site when both cosubstrates are bound, the Fe^{II} site of the Glu280Lys mutant remains six-coordinate. These results provide insight into the PAH reaction and disease mechanism at a molecular level, indicating that the first step of the mechanism is formation of a peroxy-pterin species, which subsequently reacts with the Fe^{II} site if the pterin is properly oriented for formation of an Fe−OO-pterin bridge and an open coordination position is available on the Fe^{II}.

1. Introduction

Phenylalanine hydroxylase (PAH, EC 1.14.16.1) catalyzes the rate-limiting step in phenylalanine catabolism.[1−4] Dysfunction of this enzyme in humans leads to accumulation of toxic L-Phe metabolites and severe, irreversible mental retardation through the disease phenylketonuria (PKU), which is the most common inherited disease of amino acid metabolism in the United States. PAH is one member of a family of three aromatic amino acid hydroxylases; the other two enzymes, tyrosine hydroxylase (TyrH)[3−5] and tryptophan hydroxylase (TrpH),[3,4,6] have also been linked to proper brain function.

PAH is found in the liver and exists as a homodimer or tetramer of 51.7 kDa subunits. Each subunit contains a single nonheme iron atom that must be in the Fe^{II} oxidation state for reactivity.[7−10] During the hydroxylation of L-Phe, the enzyme uses dioxygen and the tetrahydrobiopterin (BH_4) cofactor to produce L-Tyr and C4a-hydroxy-BH_2.[11] In the wild-type (WT) enzyme, this reaction is tightly coupled and the dioxygen is partitioned between the two products.[11,12] A C4a-hydroperoxy-BH_2 intermediate has been frequently proposed as an intermediate for the coupled hydroxylation reaction but has not been observed.

Both L-Phe and BH_4 have regulatory interactions with PAH in addition to their roles in the catalytic cycle. BH_4 reduces PAH from the Fe^{III} to the Fe^{II} state[13−15] while L-Phe activates the enzyme through cooperative binding to an allosteric effector site.[9,16] The formation of reduced, activated PAH is concurrent

[†] Department of Chemistry, Stanford University.
[‡] Stanford Synchrotron Radiation Laboratory.
[§] Department of Chemistry, Boston University.
[||] Department of Chemistry, Yale University.

(1) Kaufman, S. *Adv. Enzymol.* **1993**, *67*, 77−264.
(2) Kappock, T. J.; Caradonna, J. P. *Chem. Rev.* **1996**, *96*, 2659−2756.
(3) Fitzpatrick, P. F. *Annu. Rev. Biochem.* **1999**, *68*, 355−381.
(4) Fitzpatrick, P. F. *Adv. Enzymol. Relat. Areas Mol. Biol.* **2000**, *74*, 235−294.
(5) Kaufman, S. *Adv. Enzymol. Relat. Areas Mol. Biol.* **1995**, *70*, 103−220.
(6) Kuhn, D. M.; Lovenberg, W. In *Chemistry and Biochemistry of Pterins*; Blakley, R. L., Benkovic, S. J., Eds.; John Wiley & Sons: New York, 1985; Vol. 2, pp 353−382.
(7) Kaufman, S. *Adv. Enzymol.* **1971**, *35*, 245−319.
(8) Fisher, D. B.; Kirkwood, R.; Kaufman, S. *J. Biol. Chem.* **1972**, *247*, 5161−5167.
(9) Shiman, R.; Gray, D. W. *J. Biol. Chem.* **1980**, *255*, 4793−4800.
(10) Gottschall, D. W.; Dietrich, R. F.; Benkovic, S. J.; Shiman, R. *J. Biol. Chem.* **1982**, *257*, 845−849.
(11) Dix, T. A.; Bollag, G. E.; Domanico, P. L.; Benkovic, S. J. *Biochemistry* **1985**, *24*, 2955−2958.
(12) Siegmund, H.-U.; Kaufman, S. *J. Biol. Chem.* **1991**, *266*, 2903−2910.
(13) Shiman, R. *J. Biol. Chem.* **1980**, *255*, 10 029−10 032.
(14) Marota, J. J. A.; Shiman, R. *Biochemistry* **1984**, *23*, 1303−1311.
(15) Wallick, D. E.; Bloom, L. M.; Gaffney, B. J.; Benkovic, S. J. *Biochemistry* **1984**, *23*, 1295−1302.

with the appearance of a catalytically competent species. The L-Phe-induced transition from the resting, low-affinity ("tense") state (PAH^T) to the activated, high-affinity ("relaxed") state (PAH^R) has a large energetic barrier of ~34 kcal mol^{-1} (unphosphorylated enzyme) and is accompanied by a large structural rearrangement of the protein.[17]

We have previously demonstrated through the use of circular dichroism (CD), magnetic CD (MCD), and X-ray absorption spectroscopic (XAS) techniques that the resting $\{Fe^{II}\}PAH^T[\ ]$ form of the enzyme (empty brackets indicate the absence of either substrate or cofactor in the active site) is six-coordinate (6C) with a distorted octahedral geometry composed of nitrogen and oxygen ligands. Binding of either the substrate L-Phe or the cofactor analogue 5-deaza-6-methyltetrahydropterin (5-deaza-6-MPH_4) does not significantly affect the active site and neither cosubstrate binds to the Fe^{II} itself.[18,19] Binding of *both* cosubstrates, however, results in the loss of a ligand to form a five-coordinate (5C) Fe^{II} site with an open position available for dioxygen reactivity,[19,20] suggesting that a highly reactive oxygen intermediate can be generated only when both substrate and cofactor are present.[21] Extended X-ray absorption fine structure (EXAFS) analysis indicated that the ligand lost from the active site is likely a water.[20] Subsequent crystallography on truncated forms of PAH support these findings, showing a 5C Fe^{II} site when both BH_4 and a substrate analogue are bound to the catalytic domain of the protein.[22−25] The loss of a ligand to prepare the site for dioxygen reactivity is consistent with the ordered mechanism of PAH, in which the quaternary complex of $\{Fe^{II}\}PAH^R$[L-Phe, BH_4, O_2] must be formed before any product is released.[17,26,27] It is also consistent with a general mechanism observed in several nonheme ferrous enzymes, in which the resting Fe^{II} site is coordinatively saturated (6C), and binding of substrate(s) leads to the loss of a ligand and the formation of an open coordination position for O_2 to interact with the Fe^{II}.[21,28,29]

The structural insights afforded by the recent crystallographic data on PAH suggest that it is now possible to begin to understand the chemical basis for PKU/hyperphenylalaninemic (HPA) disorders. Over 280 different mutations (including missense, deletion, nonsense (termination), and splicing mutations) in the PAH gene have been characterized at the DNA level[30] and recent studies have shown that the observed clinical heterogeneity of PKU/HPA can be rationalized by this genetic heterogeneity.[31] Nevertheless, very little is known about the chemical/molecular basis of this heterogeneity. Expression analysis of the known PKU/HPA mutants can be grouped into three general categories based on their in vivo kinetic and/or stability properties:[32] (i) mutations affecting both kinetic and stability properties of PAH, (ii) kinetically perturbed mutants that are structurally stable, and (iii) mutations having normal kinetic properties but reduced stability both in vivo and in vitro. The majority of mutations that give rise to PKU/HPA disorders are found to be uniformly distributed in the catalytic iron domain (≥105), yet no mutations have been identified that involve the iron binding residues.[33]

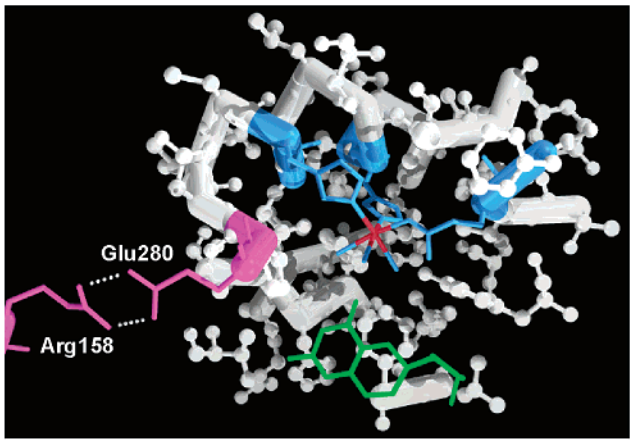

Figure 1. Iron atom is shown in red, ligands to the iron are shown in blue, oxidized pterin cofactor is shown in green, and the Arg158 and Glu280 residues are shown in magenta (left and right, respectively). Other residues shown in white are those within 10 Å of the iron atom. Figure created using PDB file 1J8U.[24]

Consequently, we have initiated spectroscopic and kinetic studies to correlate the chemical/structural basis of PKU/HPA with mechanistic changes. Two PKU-inducing mutants, Glu280Lys (E280K) and Arg158Gln (R158Q), have been expressed, purified, and characterized.[34] The Glu280 and Arg158 residues form a hydrogen-bonded pair (2.9 and 2.8 Å) in a solvent-exposed α-helix (Figure 1).[24] The R158Q mutation is associated with PKU haplotype 4 and is found primarily in German, Swiss, and Northern Italian populations.[35] It constitutes nearly 40% of all mutant haplotype 4 alleles in Europe. In vitro expression of R158Q PAH in cDNA constructs showed that mRNA levels are the same as wt PAH and immunoprecipitation results indicated that the protein is fully expressed compared to WT PAH.[36] The E280K mutation is one of the few PKU mutations that are found on multiple haplotypes: mutant haplotype 1 is found in the Danish population, haplotype 4 in the French population, and haplotype 38 in the French and Algerian populations. This mutation has an incidence of 1.5%

(16) Shiman, R.; Jones, S. H.; Gray, D. W. *J. Biol. Chem.* **1990**, *265*, 11 633−11 642.
(17) Kappock, T. J.; Harkins, P. C.; Friedenberg, S.; Caradonna, J. P. *J. Biol. Chem.* **1995**, *270*, 30 532−30 544.
(18) Loeb, K. E.; Westre, T. E.; Kappock, T. J.; Mitić, N.; Glasfeld, E.; Caradonna, J. P.; Hedman, B.; Hodgson, K. O.; Solomon, E. I. *J. Am. Chem. Soc.* **1997**, *119*, 1901−1915.
(19) Kemsley, J. N.; Mitić, N.; Zaleski, K. L.; Caradonna, J. P.; Solomon, E. I. *J. Am. Chem. Soc.* **1999**, *121*, 1528−1536.
(20) Wasinger, E.; Mitić, N.; Hedman, B.; Caradonna, J. P.; Solomon, E. I.; Hodgson, K. O. *Biochemistry* **2002**, *41*, 6211−6217.
(21) Solomon, E. I.; Brunold, T. C.; Davis, M. I.; Kemsley, J. N.; Lee, S.-K.; Lehnert, N.; Neese, F.; Skulan, A. J.; Yang, Y.-S.; Zhou, J. *Chem. Rev.* **2000**, *100*, 235−349.
(22) Flatmark, T.; Stevens, R. C. *Chem. Rev.* **1999**, *99*, 2137−2160.
(23) Erlandsen, H.; Bjørgo, E.; Flatmark, T.; Stevens, R. C. *Biochemistry* **2000**, *39*, 2208−2217.
(24) Andersen, O. A.; Flatmark, T.; Hough, E. *J. Mol. Biol.* **2001**, *314*, 279−281.
(25) Andersen, O. A.; Flatmark, T.; Hough, E. *J. Mol. Biol.* **2002**, *320*, 1095−1108.
(26) Tourian, A. *Biochim. Biophys. Acta* **1971**, *242*, 345−354.
(27) Xia, T.; Gray, D. W.; Shiman, R. *J. Biol. Chem.* **1994**, *269*, 24 657−24 665.
(28) Solomon, E. I. *Inorg. Chem.* **2001**, *40*, 3656−3669.
(29) Solomon, E. I.; Decker, A.; Lehnert, N. *Proc. Nat. Acad. Sci. U.S.A.* **2003** (in press).
(30) http://www.mcgill.ca/pahdb.
(31) Okano, Y.; Eisensmith, R. C.; Güttler, F.; Lichter-Konecki, U.; Konecki, D. S.; Trefz, F. T.; Dasovich, M.; Wang, T.; Henriksen, K.; Lou, H.; Woo, S. L. C. *New Engl. J. Med.* **1991**, *324*, 1232−1238.
(32) Flatmark, T.; Knappskog, P. M.; Bjørgo, E.; Martínez, A. In *Chemistry and Biology of Pteridines and Folates*; Pfleiderer, W., Rokos, H., Eds.; Blackwell Science: London, 1997; pp 503−508.
(33) Erlandsen, H.; Fusetti, F.; Martínez, A.; Hough, E.; Flatmark, T.; Stevens, R. C. *Nat. Str. Biol.* **1997**, *4*, 995−1000.
(34) Datta, S.; Acharya, T.; Mitić, N.; Li, H.; Caradonna, J. P., manuscript in preparation.
(35) Dworniczak, B.; Aulehle-Scholz, C.; Horst, J. *Hum. Genet.* **1989**, *84*, 95−96.
(36) Okano, Y.; Wang, T.; Eisensmith, R. C.; Steinmann, B.; Gitzelmann, R.; Woo, S. L. C. *Am. J. Hum. Genet.* **1990**, *46*, 18−25.

worldwide.[37] E280K expressed in COS cells was reported to possess immunoreactivity at 1−3%, implying low stability,[31] but expression using a pET 11d construct in *E. coli* (HMS 174) reported 100% immunoprecipitation.[38]

In this investigation, we use kinetics studies, MCD spectroscopy, and XAS to investigate the effects of the R158Q and E280K mutations on the reactivity and geometric and electronic structure of the {Fe^{II}}PAH active site.[39] The reported results offer insight into the coupled hydroxylation mechanism of PAH and contribute to our understanding of PKU/HPA at a molecular level.

2. Materials and Methods

2.1. Chemicals. All commercial reagents were of the highest grade available and were used without further purification. L-Phe, 4-morpholinepropanesulfonic acid (MOPS), and other supplies were from Sigma. Sodium dithionite and D_2O (99.9 atom % D) were from Aldrich. KCl was from Mallinckrodt. Glycerol-d_3 (98 atom % D) was obtained from Cambridge Isotopes Laboratories.

2.2. Synthesis of 5-Deaza-6-methyltetrahydropterin. The oxidized cofactor analogue 5-deaza-6-methyltetrahydropterin (5-deaza-6-MPH_4) was synthesized from 2,4-diamino-6-hydroxypyrimidine and 3-amino-2-methylacrolein following literature protocols.[40,41] The pterin was reduced over platinum dioxide following literature procedures.[42] Spectroscopic characterizations (^1H and ^{13}C NMR, UV−vis absorption) of the oxidized and reduced pterins were equivalent to those reported in the literature.[40−42]

2.3. Construction of Plasmid Vectors. Selected overexpression vectors containing PKU-inducing mutant genes of PAH were generated using standard molecular biological methods.[43] The mutants R158Q and E280K were prepared by site-directed mutagenesis of pKKPAH[17] using PCR-based techniques.[44] Oligonucleotides containing the required mutation were synthesized and used as the mutagenic primers. Primers complementary to the 5′ and 3′ ends of the coding regions of pKKPAH and containing the appropriate restriction sites were also synthesized. The PCR protocols were performed in two stages using the mutagenic primers and the flanking primers with the recombinant vector pKKPAH as template. The amplified fragments were then cloned into the corresponding restriction sites of pKKPAH using standard molecular biological techniques. The DNA sequences of the expression constructs in the region encoding the PKU rPAH mutants were obtained from both strands by automated DNA sequencing.

2.4. Bacterial Cell Growth and Protein Purification. Recombinant PKU-inducing mutant forms of PAH were overexpressed in *Escherichia coli* BL21(DE3 cells) using previously described protocols.[17,19] The purification scheme was equivalent to that described previously for WT PAH.[17] Purified enzyme was stored at −80 °C until use.

2.5. Kinetic Assays. All kinetic assays were performed on an Hewlett-Packard 8452 diode array spectrophotometer. The total iron content of the enzymes was determined by atomic absorption spectroscopy and the fraction of catalytically competent iron was measured by quantifying the formation of the catechol adduct as described previously.[17] Enzyme activity was determined using the standard PAH (Shiman) assay in which the formation of tyrosine from 1 mM L-Phe is monitored at 275 nm in the presence of 60 μM 6-methyltetrahydropterin [6-MPH_4] and 6 mM dithiothreitol in 0.1 M phosphate buffer (pH = 6.8) with 3000 units mL^{-1} catalase.[9]

Levels of 6-MPH_4 oxidation were determined by measuring the extent of 6-MPH_2 production using a coupled assay with dihydropteridine reductase (DHPR), monitoring the decrease in absorbance at 340 nm due to NADH oxidation.[45] 1.2 μM PAH enzyme and 1 mM L-Phe were incubated for 3 min at 25 °C with 0.15 mmol of NADH, an excess of DHPR, and 120 μM pterin in 0.1 M phosphate buffer (pH 6.8) with 3000 units mL^{-1} of catalase. The level of 6-MPH_4 oxidation was determined for different time periods for each of the mutants and the WT enzyme. Background levels of oxidized pterin arising from autoxidation of reduced pterin were controlled for when calculating the levels of 6-MPH_2 production.

H_2O_2 levels were determined by the method of Matsubara et al.,[46] utilizing the formation of a titanium/H_2O_2/4-(2-pyridylazo)resorcinol (Ti−PAR) mixed ligand complex that absorbs at 508 nm. Concentration-dependent curves were linear from 0 to 10 nmol of H_2O_2. Incubations were performed in 0.1 M phosphate buffer (pH = 8.0) at 25 °C for 3 min with 1.2 μM PAH, 1 mM l-Phe, 0.15 mmol of NADH, 300 μL of Ti−PAR reagent, an excess of DHPR, and 120 μM pterin. Parallel control assays, containing the same components as described above except that no enzyme was used, were routinely performed. This background peroxide production was taken into account when calculating the amount of peroxide produced during enzyme turnover.

2.6. Preparation of MCD and XAS Samples. The specific activities of the enzyme used for spectroscopic samples were 0.9 units mg^{-1} for R158Q and 0.1 units mg^{-1} for E280K where 1 unit = 1 μmol of L-Tyr min^{-1}. The active iron content per subunit was 0.84 (90% of total Fe) in R158Q, whereas that of E280K was 0.59 (91% of total Fe). Approximately 50−55 mg of protein were used for a typical spectroscopic sample.

2.6.1. Preparation of R158Q-PAH^{rest}[ ] and E280K-PAH^{rest}[ ].[47] Concentrated storage stock solutions of the appropriate enzyme samples were diluted to approximately 1 mg mL^{-1} in phenylalanine-free buffer (0.1 M MOPS and 0.3 M KCl, pH = 7.3 at 25 °C). The protein was filtered through a 0.45 μm syringe filter to remove aggregates and then concentrated in a 50 mL Amicon ultracentrifugation device over a 45 mm YM 30 membrane to a final volume of ∼2 mL. The concentrated sample was again centrifuged at 14 000 rpm for 2 min to remove any aggregates. The samples were then exchanged four times into 0.1 M MOPS, 0.3 M KCl buffer made up in D_2O and adjusted to pD 7.3 with DCl. The respective enzyme solutions were again centrifuged between the solvent exchanges to remove protein aggregates. Final protein concentrations were determined by Bradford dye binding assays. Aliquots of each sample (without glycerol-d_3) were set aside for CD experiments when appropriate. MCD samples were generated by the very slow addition of 70−75 vol % of glycerol-d_3 with careful mixing such that a homogeneous solution was formed. The resulting ≥70% glycerol-d_3 PAH solution was concentrated in a 3 mL Amicon ultrafiltration unit over a YM 30 membrane. When samples of the desired concentration were obtained, the protein was reduced anaerobically using a solution of sodium dithionite (in D_2O) freshly standardized with $K_3Fe(CN)_6$ (ferricyanide → ferrocyanide $\Delta\epsilon_{420\ nm}$ = 1020 $M^{-1}\ cm^{-1}$). The samples were frozen and then stored at −80 °C.

2.6.2. Preparation of R158Q-PAH^{act}[L-Phe, 5-deaza-6-MPH_4] and E280K-PAH^{act}[L-Phe, 5-deaza-6-MPH_4]. Concentrated storage stock solutions of the appropriate enzyme samples were diluted to approximately 1 mg mL^{-1} in 0.1 M MOPS, 0.3 M KCl buffer (pH = 7.3

(37) Byck, S.; Tyfield, L.; Carter, K.; Scriver, C. R. *Hum. Mutat.* **1997**, *9*, 316−321.
(38) Knappskog, P. M.; Eiken, H. G.; Martínez, A.; Olafsdottir, S.; Haavik, J.; Flatmark, T.; Apold, J. *Adv. Exp. Med. Biol.* **1993**, *338*, 59−62.
(39) All studies were done on {Fe^{II}}PAH unless otherwise indicated.
(40) Breitmaier, E.; Gassenmann, S. *Chem. Ber.* **1971**, *104*, 665−667.
(41) Stark, E.; Breitmaier, E. *Tetrahedron* **1973**, *29*, 2209−2217.
(42) Moad, G.; Luthy, C. L.; Benkovic, P. A.; Benkovic, S. J. *J. Am. Chem. Soc.* **1979**, *101*, 6068−6076.
(43) Maniatis, T.; Fritsch, E. F.; Sambrook, J. *Molecular Cloning: A Laboratory Manual*; Cold Spring Harbor Laboratory Press: Cold Spring Harbor, New York, 1982.
(44) Ausubel, F. M.; Brent, R.; Kingston, R. E.; Moore, D. D.; Seidman, J. G.; Smith, J. A.; Struhl, K. *Current Protocols in Molecular Biology*; Wiley-Interscience: New York, 1991; Vol. 2.
(45) Dix, T. A.; Benkovic, S. J. *Biochemistry* **1985**, *24*, 5839−5846.
(46) Matsubara, C.; Nishikawa, Y.; Yoshida, Y.; Takamura, K. *Anal. Biochem.* **1983**, *130*, 128−133.
(47) Allosteric activations in both mutants is hyperbolic as opposed to the sigmoidal behavior seen for the WT enzyme (ref 34). For this reason, we refer to the mutants as resting (PAH^{rest}) or activated (PAH^{act}) rather than using the PAH^T/PAH^R nomenclature as for WT.

at 25 °C) containing 1 mM L-Phe. The protein samples were then activated by incubation at 25 °C for 10 min. The resulting solutions were then filtered and concentrated to ~2 mL at which point additional L-Phe was added to bring the final concentration to 10 mM. 5-deaza-6-MPH_4 was similarly added in 15-fold excess to the iron content. The D_2O exchange was performed as described above except that the exchange buffer contained L-Phe.

2.7. CD and MCD Spectroscopy. Samples for CD were thawed in an N_2 atmosphere and injected into a 1 cm path length Infrasil quartz cuvette (Wilmad) adapted with a ChemGlass stopcock to prevent air oxidation during the time course of the experiment. Near-IR CD spectra (278 K, 600−2000 nm) were obtained using a Jasco J200-D spectropolarimeter with a liquid N_2-cooled InSb detector. The sample temperature was maintained at 5 °C by a recirculating water bath attached to the cell holder. Data acquisition was achieved by using routines written within the software package LabVIEW (National Instruments). Contributions to the CD intensity due to buffer and cell backgrounds were subtracted from the protein CD spectra. CD spectra of the R158Q mutant were taken with and without glycerol-d_3 to determine that the glassing agent did not affect the Fe^{II} active site (see Supporting Information, Figure S1). One sample each of R158Q-PAH^{rest}[5-deaza-6-MPH_4] with and without glycerol-d_3 were run at Fe concentrations of 1.5−2.0 mM; four samples without and three samples with glycerol-d_3 were run at Fe concentrations of 1.6−2.6 mM for R158Q-PAH^{act}[L-Phe, 5-deaza-6-MPH_4]. CD data were not collected for the E280K mutant due to sample instability.

MCD samples were thawed in an N_2 atmosphere and injected into an MCD cell assembled with a neoprene spacer (0.3 cm path length) sandwiched between two Infrasil quartz disks (Heraeus Amersil or Esco Products) and stabilized between two fitted copper plates. The sample was then quickly frozen in liquid N_2 and stored in the same until it was inserted into the cryostat under high flow of He gas. Sample numbers and Fe concentrations were as follows: four R158Q-PAH^{rest}[ ] at 1.9−2.1 mM, five R158Q-PAH^{act}[L-Phe, 5-deaza-6-MPH_4] at 1.5−2.2 mM, two E280K-PAH^{rest}[ ] at 1.2−1.5 mM, and four E280K-PAH^{act}[L-Phe, 5-deaza-6-MPH_4] at 1.6−2.0 mM. Low-temperature near-IR MCD spectra (1.6−50 K, 600−2000 nm) were obtained using the Jasco J200-D spectropolarimeter with an Oxford Instruments SM4000-7T superconducting magnet/cryostat suspended in the beam path. Depolarization of frozen samples was monitored by measuring the differential CD intensity of a nickel (+)-tartarate solution placed before and after the sample compartment.[48] MCD spectra were corrected for zero-field baseline effects induced by variability in glass quality by subtracting off the corresponding 0 T scans at each temperature. Alternatively, the directionality of the applied magnetic field was reversed and the subtracted average of the +7 T and −7 T scans, [7 − (−7)]/2 T, was used.

Spectra were fit to Gaussian band shapes using the program PeakFit (SPSS Science). Saturation magnetization data were normalized to the maximum observed intensity and fit according to published procedures to extract ground-state parameters.[49,50] Application of both negative and positive zero-field splitting models to the VTVH MCD data was used to determine the best fit.

2.8. XAS. Samples were thawed in an N_2 atmosphere and syringed into a 23 × 1 × 3 mm Lucite XAS cell with 37 μm Kapton windows. They were immediately frozen in liquid N_2 and stored in the same until loaded into an Oxford Instruments liquid helium CF1208 cryostat. Sample measurement was conducted at 10 K. Final sample concentrations were 1.8, 2.8, 1.3, and 1.6 mM for R158Q-PAH^{rest}[ ], R158Q-PAH^{act}[L-Phe, 5-deaza-6-MPH_4], E280K-PAH^{rest}[ ], and E280K-PAH^{act}[L-Phe, 5-deaza-6-MPH_4], respectively.

X-ray absorption spectra were recorded at the Stanford Synchrotron Radiation Laboratory (SSRL) on beam line 9−3.[51] Data were obtained to $k = 15$ Å^{-1} with 1 mm high in-hutch slits using internal calibration,[52] assigning the first inflection point to 7111.2 eV. The Fe K_α fluorescence data were measured using a 30-element Ge solid-state array detector with a three-wavelength Mn filter and Soller slits. Data were monitored for sample integrity by averaging sets of four successive scans and comparing a four-scan average to the previous averages. No change in the edge or EXAFS regions was observed; thus all scans of a given sample were used for a final, averaged data set including 33, 34, 34, and 32 scans for R158Q-PAH^{rest}[ ], R158Q-PAH^{act}[L-Phe, 5-deaza-6-MPH_4], E280K-PAH^{rest}[ ], and E280K-PAH^{act}[L-Phe, 5-deaza-6-MPH_4], respectively. Reduction and normalization of the averaged data were performed according to established methods.[53−56] The intensities and energies of the pre-edge features of all samples were quantified using the fitting program EDG_FIT,[57] with procedures as described in ref 20.

Theoretical EXAFS signals, $\chi(k)$, were calculated using FEFF (version 6) and the crystal structure as a starting model. The model was fit to the EXAFS data using EXAFSPAK.[58] The structural parameters R, the bond distance in Å, and σ^2, the bond variance in Å^2 were varied in the fits of each sample. The threshold energy in eV ($k = 0$, E_0), was kept to a common, variable (ΔE_0) value relative to 7130 eV for all components within a given fit of a sample. Fits were evaluated by comparing the normalized error for each fit, F, and by visual inspection of the fits to the EXAFS data and the respective Fourier transforms. Although the first coordination spheres for the PAH samples do not have solely nitrogen ligation, distinguishing between nitrogen and oxygen backscatterers is not possible; therefore, all first coordination sphere components were fit with nitrogen phases and amplitudes. More distant second shell single scattering and multiple scattering waves were fit with carbon components from FEFF. For preliminary fitting, outer shell single- and multiple scattering paths were linked together at input model distances with the respective first coordination sphere component. Debye−Waller factors were set to initial values of 0.005 00 Å^2 and allowed to float in all fits. In the final fits, the distance link was released and all components were allowed to float. In all cases, the outer shell components moved very little (<0.05 Å) from their linked positions. On the basis of studies of complexes of known structures, the uncertainties in final distances are within 0.02 Å. The total coordination number was obtained from pre-edge analysis (vide infra) and not varied; however, the distribution of ligands into shorter or longer components was varied in integer steps to determine the best fit.

3. Results and Analysis

3.1. Kinetics. 3.1.1. Investigation of Product/Cofactor Coupling for WT and PKU-Inducing PAH. Oxidation of the redox active cofactor required for PAH activity is tightly coupled to formation of product, L-Tyr, during normal enzyme-

(48) Browett, W. R.; Fucaloro, A. F.; Morgan, T. V.; Stephens, P. J. *J. Am. Chem. Soc.* **1983**, *105*, 1868−1872.
(49) Solomon, E. I.; Pavel, E. G.; Loeb, K. E.; Campochiaro, C. *Coord. Chem. Rev.* **1995**, *95*, 369−460.
(50) Pavel, E. G.; Kitajima, N.; Solomon, E. I. *J. Am. Chem. Soc.* **1998**, *120*, 3949−3962.
(51) Ring conditions: 3 GeV, 50−100 mA. Beam line conditions: Rh-coated pre-monochromator, harmonic rejection and collimation mirror; 111 keV cutoff; Si(220) double-crystal monochromator fully tuned; cylindrical bent Rh-coated focusing post-monochromator mirror; energy resolution <1.4 eV.; edge position reproducibility <0.2 eV.
(52) Scott, R. A.; Hahn, J. E.; Doniach, S.; Freeman, H. C.; Hodgson, K. O. *J. Am. Chem. Soc.* **1982**, *104*, 5364−5369.
(53) Cramer, S. P.; Hodgson, K. O. *Prog. Inorg. Chem.* **1979**, *25*, 1−39.
(54) Scott, R. A. *Methods Enzymol.* **1985**, *117*, 414−459.
(55) DeWitt, J. G.; Bentsen, J. G.; Rosenzweig, A. C.; Hedman, B.; Green, J.; Pilkington, S.; Papaefthymiou, G. C.; Dalton, H.; Hodgson, K. O.; Lippard, S. J. *J. Am. Chem. Soc.* **1991**, *113*, 9219−9235.
(56) Zhang, H. H.; Hedman, B.; Hodgson, K. O. In *Inorganic Electronic Structure and Spectroscopy*; Solomon, E. I., Lever, A. B. P., Eds.; John Wiley & Sons: New York, 1999; pp 513−554.
(57) George, G. N. EDG_FIT; Stanford Synchrotron Radiation Laboratory, Stanford Linear Accelerator Center, Stanford University, Stanford, CA 94309.
(58) George, G. N. EXAFSPAK; Stanford Synchrotron Radiation Laboratory, Stanford Linear Accelerator Center, Stanford University, Stanford, CA 94309.

Table 1. Cofactor/Product Coupling versus H_2O_2 Production during Enzyme Turnover

	Tyr[a]	NADH (= total pterin)[a]	Tyr/NADH (= coupling)	released H_2O_2[a,b]	mass balance[c]
WT	1925 ± 14	1950 ± 50	0.98	40 ± 25	101 ± 3
R158Q	1110 ± 19	4790 ± 65	0.23	3920 ± 40	105 ± 2
E280K	855 ± 15	4750 ± 59	0.18	4160 ± 30	105 ± 2

[a] All amounts are in nmol and are normalized with respect to active Fe. Measurements are for 8 s. [b] Background production of H_2O_2 was determined to be 1680 ± 10 in the absence of PAH; values in the table are corrected for this background amount. [c] Total production of Tyr + H_2O_2, expressed as a percentage of NADH consumption.

catalyzed reactions.[45] A second pathway, however, also exists that involves the direct oxidation of tetrahydropterins (PH_4) to quinonoid dihydropterins (q-PH_2), producing H_2O_2. This uncoupled pathway in WT PAH is nonproductive with respect to product formation and does not proceed through the formation of the C4a-hydroxy-PH_2 species.[45] The partitioning of cofactor utilization between coupled and uncoupled pathways was examined using parallel assays designed to quantify production of both L-Tyr and oxidized 6-MPH_4. Results of these experiments for WT PAH and the R158Q and E280K mutants are shown in Table 1. Each reaction was performed in triplicate and under cofactor-limiting conditions. Control reactions utilizing WT PAH indicate that oxidation of the synthetic cofactor 6-MPH_4 is tightly coupled to hydroxylation of L-Phe to L-Tyr (98% coupled). A comparison of 6-MPH_4 consumption (based on NADH utilization) as compared to tyrosine formation for the R158Q mutant shows a significant decrease in cofactor coupling (to 23%) in addition to a diminished specific activity of the mutant enzyme (6.1 μmol Tyr min^{-1} mg^{-1} for WT PAH vs 0.9 μmol Tyr min^{-1} mg^{-1} for R158Q PAH). Although a comparable decrease in cofactor coupling is observed for the E280K mutant versus WT PAH (18% coupled), there is an approximate 60-fold decrease in the specific activity (6.1 μmol Tyr min^{-1} mg^{-1} for WT PAH vs 0.1 μmol Tyr min^{-1} mg^{-1} for E280K PAH).

The observation that both PKU-inducing mutant enzymes exhibit less hydroxylation of substrate than 6-MPH_4 oxidation suggests the operation of at least two pathways for the reaction of cofactor with dioxygen. These results are analogous to previous studies in which the use of alternative substrates or cofactor analogues resulted in uncoupling during PAH turnover.[2,59] Table 1 also indicates that the rate of 6-MPH_4 oxidation is greater for the PKU-inducing mutant enzymes than for the control reaction with WT PAH (4.3-fold increase in R158Q and 5.5-fold in E280K). Because the R158Q and E280K enzymes are less effective hydroxylating enzymes than WT PAH, these data suggest that the rate of 6-MPH_4 oxidation in the uncoupled pathway is greater than the rate of 6-MPH_4 oxidation in the tightly coupled pathway.

3.1.2. H_2O_2 Production during Enzyme Turnover. During uncoupled reactions, reduced pterin utilization beyond that necessary for the hydroxylation of substrate is converted to the q-PH_2 state with the concomitant transfer of electrons and protons to dioxygen generating H_2O_2. Parallel assays were therefore performed in which the levels of H_2O_2 were directly measured and compared to both reduced pterin usage and tyrosine production over the same time period (8 s). As shown in Table 1, only trace amounts of H_2O_2 (2%) were observed in control reactions with WT PAH. In contrast, hydrogen peroxide production is significant in the reactions of both R158Q and E280K. This is unlike the uncoupling process observed for p-Cl−Phe (35% coupled) or PH_4 (56% coupled), in which a lack of significant levels of H_2O_2 were reported.[45] Table 1 also shows that the molar quantities of NADH utilized for each enzyme system equals, within experimental errors, the moles of L-Tyr and H_2O_2 produced. These data indicate that the uncoupled pterin oxidations give rise to H_2O_2 and that the peroxide leaves the active site and is detected prior to background reactions that may involve the breakdown of H_2O_2 to hydroxyl radicals,[45] which are proposed to be the species responsible for PAH inactivation.

3.2. MCD Spectroscopy. The ^5D ground state for the d^6 Fe^{II} free ion is split under octahedral symmetry into a $^5T_{2g}$ ground state (d_{xz}, d_{yz}, d_{xy}) and a ^5E_g excited state (d_{z^2}, $d_{x^2-y^2}$), separated by $10Dq \approx 10\,000$ cm^{-1} for oxygen and nitrogen ligands. The splitting of the ^5E_g excited state, Δ^5E_g, is sensitive to the coordination number and geometry of the Fe^{II} site and transitions to these orbitals can be observed in near-IR CD and MCD spectroscopy.[21,28,49] Model studies have shown that 6C distorted octahedral Fe^{II} sites have two transitions centered at ~10 000 cm^{-1} with $|\Delta^5E_g| \approx 2000$ cm^{-1}, 5C sites have two transitions at ~10 000 cm^{-1} and ~5000 cm^{-1} with $|\Delta^5E_g| \approx 5000$ cm^{-1}, and 4C sites have two transitions in the region of 4000−7000 cm^{-1}.[50] For 5C sites, the two transitions shift from higher to lower energy as geometry changes from trigonal bipyramidal to square pyramidal.

The temperature and field dependence of these transitions is characterized by the nesting (nonsuperimposing behavior) of isotherms when MCD intensity is plotted versus $\beta H/2kT$ and can be used to gain insight into the ground-state electronic structure of Fe^{II} sites.[21,28,49] For systems with negative zero-field splitting (−ZFS; $D < 0$) this behavior is due to the rhombic zero-field splitting (δ) of the $M_S = \pm 2$ doublet ground state. For systems with positive zero-field splitting (+ZFS; $D > 0$), similar nesting arises from off-axis Zeeman mixing of a pseudo-doublet ground-state comprising the $M_S = 0$ and one component of the $M_S = \pm 1$ sublevels. In general, $-D$ and $+D$ systems can be distinguished by much larger nesting behavior observed for $+D$ cases (split by $\sim D$ instead of δ) and the presence of a low-lying singlet excited state (the other component of $M_S = \pm 1$).

Ground state parameters are obtained for both systems by computationally fitting the experimental VTVH MCD data to an orientation-averaged intensity expression that includes the rhombic and Zeeman splitting of a non-Kramers doublet (δ and $g_{||}$) as well as the transition polarization ratio (M_z/M_{xy}) and contributions from linear temperature-independent ***B***-terms and low-lying excited states.[21,28,49] The results obtained from this analysis are directly related to the splitting of the $^5T_{2g}$ ground state so that the orbital splittings may be determined ($\Delta \equiv d_{xz,yz} - d_{xy}$; $V \equiv d_{xz} - d_{yz}$).

The MCD spectrum of R158Q-PAH^{rest}[ ] is shown in blue in Figure 2A. The Gaussian fit of the spectrum indicates that two transitions at 8730 and 10 700 cm^{-1} are needed to fit the spectrum (Table 2 and Supporting Figure S2A). The pattern of two transitions centered at ~10 000 cm^{-1} and split by ~2000

(59) Shiman, R. In *Chemistry and Biochemistry of Pterins*; Blakley, R. L., Benkovic, S. J., Eds.; John Wiley & Sons: New York, 1985; Vol. 2, pp 179−249.

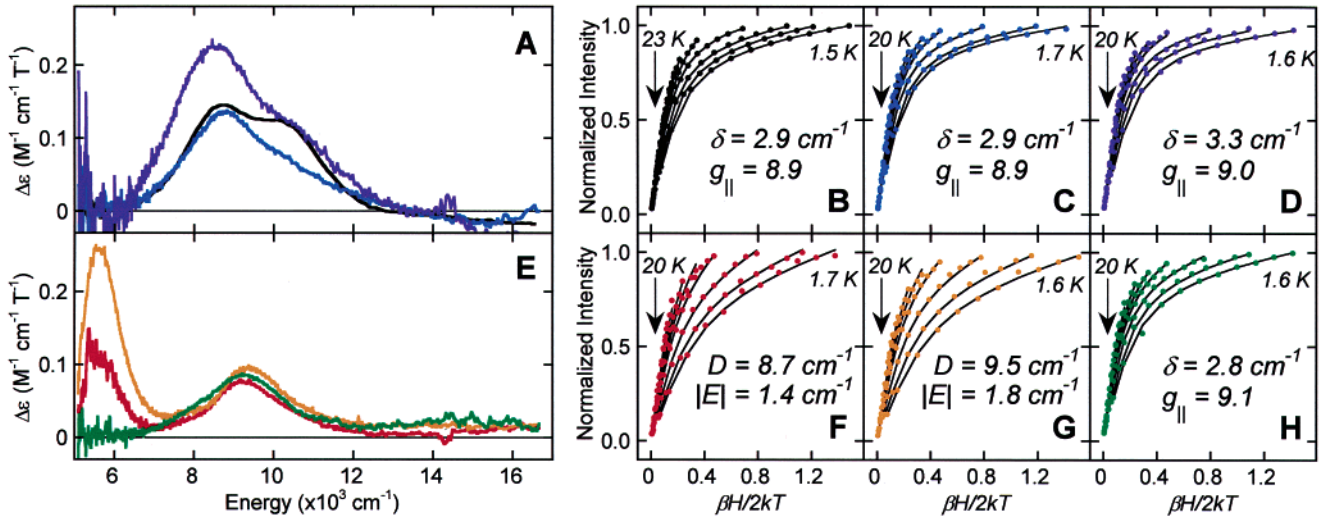

Figure 2. MCD spectra and saturation data for WT (black), R158Q (blue), and E280K (purple) $PAH^{T/rest}$[ ]; and WT (red), R158Q (orange), and E280K (green) $PAH^{R/act}$[L-Phe, 5-deaza-6-MPH_4]. The MCD data shown in parts A and E were collected at 5 K and 7 T. The VTVH data shown in B−D and F−H were collected at fixed temperatures of 1.5−1.7 K, 2.0−2.1, 3, 5, 7, 10, 15, 20, 30, and 50 K and a series of fixed fields for the following wavelengths: (B) 8500 cm^{-1}, (C) 8930 cm^{-1}, (D) 8570 cm^{-1}, (F) 6055 cm^{-1}, (G) 5970 cm^{-1}, and (H) 9365 cm^{-1}. Data for temperatures >25 K are not shown for clarity. Error bars are typically twice the size of the symbol used. The data are in colored circles and the fits to the data using the parameters in Table 2 are shown as solid black lines. WT data are taken from refs 18 and 19.

Table 2. Ligand Field Transition Energies and Ground State Parameters

	band 1[a]	band 2[a]	10*Dq*[a]	Δ^5E_g[a]	δ[a]	$g_{\|\|}$	Δ[a]	$\|V\|$[a]
WT^T[ ][b]	8500	10 300	9400	1600	2.9	8.9	−250	70
WT^R[L-Phe, 5-deaza-6-MPH_4]	5200	9280	7240	4080	5.2	8.0	+825	315
$R158Q^{rest}$[ ]	8730	10 700	9720	1970	2.9	8.9	−200	55
$R158Q^{act}$[L-Phe, 5-deaza-6-MPH_4]	5630	9440	7540	3810	5.1	8.0	+750	360
$E280K^{rest}$[ ]	8500	10 600	9550	2100	3.3	9.0	−200	60
$E280K^{act}$[L-Phe, 5-deaza-6-MPH_4]	9100	10 800	9950	1700	2.8	9.1	−250	70

[a] Values in cm^{-1}. [b] WT values taken from refs 19 and 18.

cm^{-1} is consistent with a distorted octahedral Fe^{II} site.[21,28,49,50] The spectrum of R158Q-PAH^{rest}[ ] is very similar to that of WT PAH^T[ ] (Figure 2A, black),[18] with a small perturbation evident from the decreased intensity of the band at higher energy. This intensity difference can be attributed to a change in polarization of the transition. VTVH MCD data for R158Q-PAH^{rest}[ ] are shown in Figure 2C and fit with ground-state parameters of $\delta = 2.9$ cm^{-1}, $g_{||} = 8.9$, $\Delta = -200$ cm^{-1}, and $|V| = 55$ cm^{-1}. These parameters are consistent with a $-D$ system and are identical to those determined for the WT PAH^T[ ] (Figure 2B and Table 2).[18] Together, the excited state and ground-state parameters indicate that the R158Q mutation has no effect on the resting 6C active site of PAH^T[ ].

Figure 2E shows the MCD spectrum of R158Q-PAH^{act}[L-Phe, 5-deaza-6-MPH_4] in orange. In this case, we observe only one band at ~10 000 cm^{-1} (9440 cm^{-1}) while the second band is at 5630 cm^{-1} (Gaussian fit shown in Supporting Figure S2B). This gives $|\Delta^5E_g| = 3810$ cm^{-1} and is consistent with a square pyramidal 5C site.[21,28,49,50] Binding of both cosubstrates therefore results in the loss of a ligand, leaving an open coordination position on the Fe^{II} atom. The loss of a ligand to form a 5C site is also observed in WT PAH^R[L-Phe, 5-deaza-6-MPH_4] (Figure 2E, red);[19] however, for the R158Q mutant the lower energy band is at a higher energy as compared to the WT spectrum. Using the shape and intensity obtained from the Gaussian fit of the lower-energy R158Q band to model the shoulder seen for WT PAH^R[L-Phe, 5-deaza-6-MPH_4], we get values of $10Dq = 7240$ cm^{-1} and $\Delta^5E_g = 4080$ cm^{-1} for WT PAH^R[L-Phe, 5-deaza-6-MPH_4] (Table 2). These are comparable to the values obtained for the R158Q mutant ($10Dq = 7540$ cm^{-1} and $\Delta^5E_g = 3810$ cm^{-1}) and, as with the resting enzyme, indicate that the Fe^{II} site with both cosubstrates bound has not been substantially affected by the mutation. The shift of the lower energy band by ~400 cm^{-1} is likely due to a slight strengthening of the axial ligand in the R158Q mutant, which raises the energy of the d_{z^2} orbital.

The saturation data for R158Q-PAH^{act}[L-Phe, 5-deaza-6-MPH_4] show a dramatic increase in nesting when both cosubstrates are bound as compared to the resting enzyme (Figure 2G vs 2C). This is indicative of a +ZFS ($+D$) system[21,28,49] whereas the resting site has −ZFS ($-D$). Analysis of these data yields essentially identical ground state parameters as previously determined for the WT PAH^R[L-Phe, 5-deaza-6-MPH_4] site−$\delta = 5.1$ cm^{-1}, $g_{||} = 8.0$, $\Delta = +750$ cm^{-1}, and $|V| = 360$ cm^{-1}−once again indicating that the mutation of Arg158 to Gln does not affect the Fe^{II} active site of the enzyme either in its resting state or with both cosubstrates bound.

The purple spectrum in Figure 2A is the E280K-PAH^{rest}[ ] species. Two Gaussian bands are required to fit the spectrum (Table 2 and Supporting Figure S2C) with energies, 10*Dq*, and Δ^5E_g all similar to both WT PAH^T[ ] and R158Q-PAH^{rest}[ ]. The saturation data for E280K-PAH^{rest}[ ] are shown in Figure 2D. Visually, the nesting appears to be very similar to the resting states of the WT enzyme and R158Q mutant, and the ground-state parameters are the same within error (Table 2). Clearly, neither mutation has a significant effect on the Fe^{II} site of the resting enzyme with no cosubstrates bound.

In contrast, the spectrum of E280K-PAH^{act}[L-Phe, 5-deaza-6-MPH_4] is shown in Figure 2E (green) and is quite different from either WT PAH^R[L-Phe, 5-deaza-6-MPH_4] or R158Q-PAH^{act}[L-Phe, 5-deaza-6-MPH_4]. The lower-energy "5C" band is no longer present and the peak at ~9500 cm^{-1} is wider and

less symmetric. Two transitions at 9100 cm^{-1} and 10 800 cm^{-1} are required to fit the spectrum, indicating that this site is 6C with a distorted octahedral geometry. The transition energies, 10*Dq*, and Δ^5E_g all indicate that the site is similar to the resting form of the enzyme (Table 2). Figure 2H shows the saturation data for the E280K-PAH^{act}[L-Phe, 5-deaza-6-MPH$_4$] species. The nesting of the isotherms also appears to be very similar to the resting E280K-PAH^{rest}[ ], while the fit parameters are the same within error and are nearly identical to WT PAH^T[ ]: $\delta = 2.8$ cm^{-1}, $g_{||} = 9.1$, $\Delta = -250$ cm^{-1}, and $|V| = 70$ cm^{-1}. The E280K mutation therefore affects the binding of either or both of L-Phe and pterin cofactor such that the 6C→5C conversion seen in the WT enzyme upon binding of cosubstrates does not occur.

3.3. XAS. 3.3.1. Pre-edge Analysis. Model studies have shown that pre-edge shape and intensity patterns can be correlated to coordination number and geometry.[60,61] The 1s→3d pre-edge features are formally electric dipole forbidden but gain intensity through the weaker electric quadrupole transition, and are therefore observed to be weak in centrosymmetric complexes.[61] Typical 6C ferrous complexes have a pre-edge intensity of ~4 units distributed over three features split by ~2 eV. It has been shown, however, that loss of centrosymmetry results in additional pre-edge intensity due to 4p orbital mixing into the unoccupied and half-occupied 3d orbitals.[60] Because the 1s→4p electric dipole transition is ~100-fold more efficient than the quadrupole transition, only a few percent 4p mixing is necessary to greatly enhance the intensity of the pre-edge feature. Noncentrosymmetric complexes are therefore observed to have a higher pre-edge intensity; 5C and tetrahedral ferrous models are well fit by two features having ~12 and ~13 units of intensity, respectively. Although the intensities of the 5C and 4C noncentrosymmetric complexes are similarly large, the sites are differentiated by their respective intensity distributions.[61] Protein active sites with dissimilar ligation, variations in bond distances, and noncoincidence of the molecular axes with any of the ligands' bonding orbitals will therefore have an increased pre-edge intensity relative to models with similar oxidation state and geometry due to the additional 1s→4p dipole contribution to the pre-edge.

The pre-edge energies and intensities for the individual features of the R158Q-PAH^{rest}[ ], R158Q-PAH^{act}[L-Phe, 5-deaza-6-MPH$_4$], E280K-PAH^{rest}[ ] and E280K-PAH^{act}[L-Phe, 5-deaza-6-MPH$_4$] complexes are listed in Table 3 and the data are shown in Figure 3. The pre-edge features of R158Q-PAH^{rest}[ ] (blue), E280K-PAH^{rest}[ ] (purple), and E280K-PAH^{act}[L-Phe, 5-deaza-6-MPH$_4$] (green) are all strikingly similar in pre-edge shape and intensity, whereas the pre-edge of the R158Q-PAH^{act}[L-Phe, 5-deaza-6-MPH$_4$] complex (orange) is significantly higher in intensity. Each complex consists of at least two features as seen from the second derivative of the data (Figure 3, inset). The pre-edge data and second derivatives of the data for the WT PAH^T[ ] and PAH^R[L-Phe, 5-deaza-6-MPH$_4$] are reproduced from ref 20 and also shown in Figure 3 (black and red spectra, respectively).

Two features at 7111.8 and 7113.6 eV with intensities of 5.6 and 3.6 units, respectively, adequately reproduced the pre-edge data and the second derivative of the data for the R158Q-PAH^{rest}[ ] complex. The total pre-edge area of 9.2 units is greater than that of typical 6C model complexes, but significantly less than that of 5C models.[61] Deviations from a strict octahedral field in protein active sites can promote 4p mixing into the d-orbitals, and typically give rise to pre-edge areas greater than those for octahedral model complexes.[18,62,63] The shape and total intensity of the R158Q-PAH^{rest}[ ] pre-edge data is extremely similar to that found for the WT PAH^T[ ] complex (Figure 3, blue vs black), which has been characterized as having a 6C active site.[18,20] Thus, from the pre-edge analysis the R158Q-PAH^{rest}[ ] active site is 6C and is likely very similar to that of the WT resting enzyme.

The pre-edge data and the second derivative of the data for the R158Q-PAH^{act}[L-Phe, 5-deaza-6-MPH$_4$] complex are adequately reproduced by two features at 7111.8 and 7113.5 eV with intensities of 8.5 and 5.6 units, respectively (Table 3). The total pre-edge area of 14.1 units is comparable to that of 5C models, where the increased pre-edge intensity of the low energy feature is indicative of the additional 4p mixing into the d_{z^2} orbital of a square pyramidal site.[61] The shape and total intensity of the R158Q-PAH^{act}[L-Phe, 5-deaza-6-MPH$_4$] pre-edge data is extremely similar to that found for the WT PAH^R[L-Phe, 5-deaza-6-MPH$_4$] complex (Figure 3, orange vs red), which has been characterized as having a 5C active site.[19,20] Thus, from the pre-edge analysis the R158Q-PAH^{act}[L-Phe, 5-deaza-6-

Table 3. XAS Pre-edge Energies and Intensities

	energy (eV)	area	energy (eV)	area	total area
WT^T[ ]^a	7111.8^b	5.1^b	7113.6	3.0	8.1
WT^R[L-Phe, 5-deaza-6-MPH$_4$]^a	7111.7	8.6	7113.5	5.3	13.9
R158Q^{rest}[ ]	7111.8	5.6	7113.6	3.6	9.2
R158Q^{act}[L-Phe, 5-deaza-6-MPH$_4$]	7111.8	8.5	7113.5	5.6	14.2
E280K^{rest}[ ]	7111.8	5.6	7113.6	4.0	9.6
E280K^{act}[L-Phe, 5-deaza-6-MPH$_4$]	7111.9	6.4	7113.6	3.5	9.9

^{a} WT fit values taken or adapted from ref 20. ^{b} Energy is the intensity-weighted average of the first two peaks of WT^T[ ]; area is the combined areas of the two peaks.

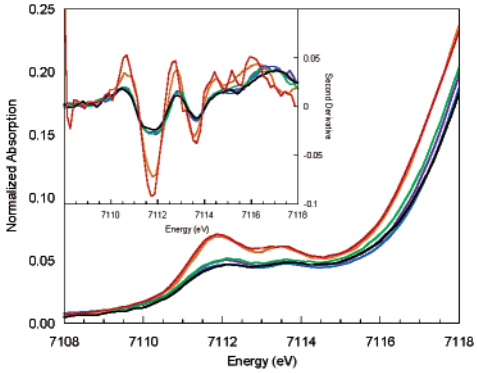

Figure 3. Pre-edge spectra of WT (black), R158Q (blue), and E180K (purple) PAH$^{T/rest}$[ ]; and WT (red), R158Q (orange), and E280K (green) PAH$^{R/act}$[L-Phe, 5-deaza-6-MPH$_4$]. The second derivative of the data is shown in the inset. WT data are taken from refs 18 and 20.

(60) Randall, C. R.; Shu, L.; Chiou, Y.-M.; Hagen, K. S.; Ito, M.; Kitajima, N.; Lachicotte, R. J.; Zang, Y.; Que, L., Jr. *Inorg. Chem.* **1995**, *34*, 1036−1039.
(61) Westre, T. E.; Kennepohl, P.; DeWitt, J. G.; Hedman, B.; Hodgson, K. O.; Solomon, E. I. *J. Am. Chem. Soc.* **1997**, *119*, 6297−6314.
(62) Shu, L.; Chiou, Y.-M.; Orville, A. M.; Miller, M. A.; Lipscomb, J. D.; Que, L., Jr. *Biochemistry* **1995**, *34*, 6649−6659.
(63) Davis, M. I.; Wasinger, E. C.; Westre, T. E.; Zaleski, J. M.; Orville, A. M.; Lipscomb, J. D.; Hedman, B.; Hodgson, K. O.; Solomon, E. I. *Inorg. Chem.* **1999**, *38*, 3676−3683.

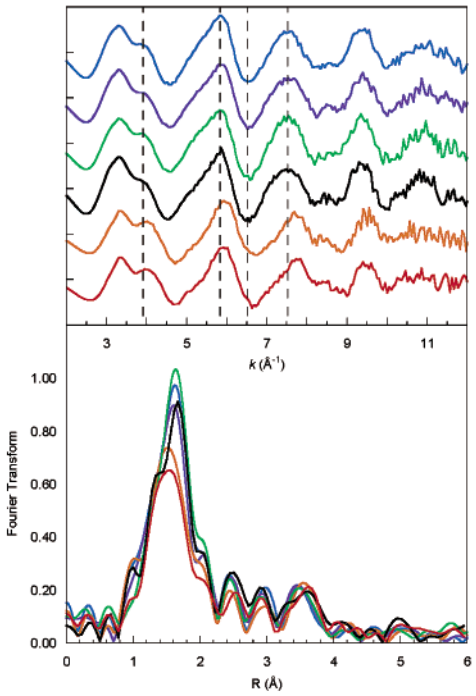

Figure 4. EXAFS (top) and Fourier transform (bottom) of the data for WT (black), R158Q (blue), and E180K (purple) PAH$^{T/rest}$[ ]; and WT (red), R158Q (orange), and E280K (green) PAH$^{R/act}$[L-Phe, 5-deaza-6-MPH$_4$]. WT data are taken from refs 18 and 20.

MPH$_4$] active site is 5C and very similar to that of the WT PAH^{R}[L-Phe, 5-deaza-6-MPH$_4$] enzyme.

Two features are required to fit the pre-edge data and second derivative of the data for the E280K-PAH^{rest}[ ] complex (Table 3). With 5.6 units of intensity at 7111.8 eV and 4.0 units of intensity at 7113.6 eV, the E280K-PAH^{rest}[ ] complex is similar in shape and intensity to the pre-edges of both R158Q-PAH^{rest}[ ] and WT PAH^{T}[ ].

Similarly, two features are required to fit the pre-edge data and second derivative of the data of E280K-PAH^{act}[L-Phe, 5-deaza-6-MPH$_4$] at 7111.9 and 7113.6 eV with 6.4 and 3.5 units of intensity, respectively (Table 3). The pre-edge shape and intensity pattern are extensively altered relative to those of the WT PAH^{R}[L-Phe, 5-deaza-6-MPH$_4$] and the total intensity of 9.9 units is much less. The pre-edge of E280K-PAH^{act}[L-Phe, 5-deaza-6-MPH$_4$] is very similar, however, to that of E280K-PAH^{rest}[ ], R158Q-PAH^{rest}[ ], and WT PAH^{T}[ ] (Figure 3), and is therefore described as having a distorted octahedral active site. Thus, from the pre-edge analysis, the E280K mutation has caused a significant change of the active site behavior relative to the WT enzyme upon binding of both cosubstrates.

3.3.2. XAS EXAFS. The EXAFS data were measured to $k = 15$ Å^{-1}; however, the fits to the data were limited to the range $k = 2.0-12.0$ Å^{-1} according to the quality of the data averages. Differences in the overall phase and amplitude are seen in the EXAFS and Fourier transformed data (Figure 4). The R158Q-PAH^{act}[L-Phe, 5-deaza-6-MPH$_4$] oscillations (orange) are shifted to lower *k*-frequency, indicating a shorter average distance, and are lower in amplitude than the EXAFS of R158Q-PAH^{rest}[ ] (blue), E280K-PAH^{rest}[ ] (purple), and E280K-PAH^{act}[L-Phe, 5-deaza-6-MPH$_4$] (green), which are all very similar to one another. This is also clearly seen in the Fourier transforms of the data (Figure 4, bottom), for which the primary disparity between R158Q-PAH^{act}[L-Phe, 5-deaza-6-MPH$_4$] and the other samples is an ~20% greater intensity in the first coordination sphere Fourier transform peak for the other samples. Although slight differences in Fourier transform peak intensity are observed between R158Q-PAH^{rest}[ ], E280K-PAH^{rest}[ ], and E280K-PAH^{act}[L-Phe, 5-deaza-6-MPH$_4$], none of these differences are nearly as great as those between R158Q-PAH^{act}[L-Phe, 5-deaza-6-MPH$_4$] and the other three samples.

Table 4. EXAFS Fits

fit no.	sample		CN	R (Å)	σ^2 (Å^2)	F[b]
	WT^{T}[ ][a]	Fe−O	1	1.97	.00427	.216
		Fe−N/O	5	2.14	.00437	
		Fe−C SS	5	3.08	.00507	
		Fe−C MS	8	4.36	.00385	
	WT^{R}[L-Phe, 5-deaza-6-MPH$_4$][a]	Fe−O	1	1.94	.00300	.232
		Fe−N/O	4	2.10	.00534	
		Fe−C SS	5	3.07	.00725	
		Fe−C MS	8	4.30	.00558	
1	R158Q^{rest}[ ]	Fe−O	1	1.96	.00732	.145
		Fe−N/O	5	2.12	.00502	
		Fe−C SS	5	3.08	.00788	
		Fe−C MS	8	4.38	.00447	
2	R158Q^{act}[L-Phe, 5-deaza-6-MPH$_4$]	Fe−O	1	1.92	.00111	.268
		Fe−N/O	4	2.09	.00389	
		Fe−C SS	5	3.06	.00995	
		Fe−C MS	8	4.33	.00416	
3	E280K^{rest}[ ]	Fe−O	1	1.96	.00459	.166
		Fe−N/O	5	2.12	.00512	
		Fe−C SS	5	3.06	.00802	
		Fe−C MS	8	4.35	.00367	
4	E280K^{act}[L-Phe, 5-deaza-6-MPH$_4$]	Fe−O	1	1.96	.00567	.219
		Fe−N/O	5	2.13	.00430	
		Fe−C SS	5	3.07	.00744	
		Fe−C MS	8	4.37	.00338	

[a] WT fit values from ref 20. [b] $F = \Sigma[(\chi_{exp} - \chi_{obsd})^2 k^6]/\Sigma[\chi_{exp}^2 k^6]$.

From the pre-edge and MCD results, R158Q-PAH^{rest}[ ] is 6C and therefore EXAFS fits were restricted to a total first coordination sphere of six ligands. Modeling the EXAFS data with one N/O atom at 1.96 Å and 5 N/O atoms at 2.12 Å (Table 4, fit 1) adequately fits the EXAFS data and the Fourier transform of the data. It should be noted that although the Debye−Waller value of the 1.96 Å component is marginally high, reducing σ^2 by 30% and floating the remaining parameters does not appreciably change the error value, distances, or the σ^2 values of the other parameters. Furthermore, an EXAFS fit using only a single contribution of six N/O backscatterers leads to an average first shell distance of 2.11 Å, a significantly higher error value, and a worse visual fit to the Fourier transform. A split first shell is therefore necessary to fit the EXAFS data of R158Q-PAH^{rest}[ ]. Modeling the EXAFS with two short ligands and four longer ligands produces a fit with σ^2 values too high for two ligands at a short distance. Attempts to include a shell of ligands at a distance longer than 2.15 Å were unsuccessful. The EXAFS data required two additional components to fit the outer shell carbon single- and multiple-scattering from the histidine and glutamate ligands of R158Q-PAH^{rest}[ ] as listed in Table 4. A comparison of the best fit to the R158Q-PAH^{rest}[ ] EXAFS data with the EXAFS results obtained from WT PAH^{T}[ ] indicate that these two sites are quite similar (Table 4), therefore little or no change is introduced by the R158Q mutation when the cosubstrates are not present.

The EXAFS of R158Q-PAH^{act}[L-Phe, 5-deaza-6-MPH$_4$] (Figure 4, top, orange data) is also shifted to lower frequency indicating a shorter average bond distance, which is consistent with MCD and pre-edge analyses that indicate the active site is 5C. An EXAFS fit using only a single contribution of six nitrogen backscatterers leads to an average first shell distance of 2.07 Å, a relatively high fit value, and a large σ^2 value. Using two contributions to fit the first coordination sphere, one ligand at 1.92 Å and 4 ligands at 2.09 Å, results in a significant lowering of the error value and reasonable σ^2 values for both components (Table 4, fit 2). Two additional components are required to fit the outer shell carbon single- and multiple-scattering from the histidine and glutamate ligands. Notably, the first shell Fourier transform intensity is significantly reduced relative to the R158Q-PAH^{rest}[ ] form, yet the intensity in the distant single scattering and multiple scattering region (3.0−5.0 Å) is largely unaffected. Thus, the ligand that is absent in the R158Q-PAH^{rest}[ ] sample must have little or no multiple scattering components. The short component in the EXAFS fit is ascribed to the lone anionic glutamate ligand and consequently cannot be the ligand lost upon binding of cosubstrates. Attempting to fit the multiple scattering region using coordination numbers that reflect the loss of a histidine from the active site results in unreasonably low or negative σ^2 values for the multiple scattering components. Therefore, the ligand lost must be a water molecule and the likely remaining ligation is comprised of two histidine ligands, a bidentate glutamate, and one water molecule. This is extremely similar to the results obtained for WT PAH^R[L-Phe, 5-deaza-6-MPH$_4$] (Table 4).

EXAFS fits to E280K-PAH^{rest}[ ] were restricted to a total first coordination sphere of six ligands in accordance with pre-edge and MCD results (vide infra). Similar to the R158Q-PAH^{rest}[ ] data, a split coordination sphere is required to fit the EXAFS of E280K-PAH^{rest}[ ], with one nitrogen atom at 1.96 Å and five nitrogen atoms at 2.12 Å (Table 4, fit 3). First shell components longer than 2.15 Å could not be fit in the data retaining reasonable σ^2 values. Carbon single- and multiple-scattering components complete the fit to the data. This fit is extremely similar to the results of fitting WT PAH^T[ ] indicating that the E280K mutation has little effect on the geometric structure of the active site.

Binding of the L-Phe and 5-deaza-6-MPH$_4$ cosubstrates to E280K-PAH^{rest}[ ] results in little change to the EXAFS or Fourier transform (Figure 4, purple vs green). Pre-edge and MCD results indicate a 6C active site, and therefore EXAFS fits were restricted to a total coordination number of six. Using a single contribution of six nitrogen ligands results in an average distance of 2.12 Å. The EXAFS data can be fit more adequately using a split first shell of one ligand at 1.96 Å and five ligands at 2.13 Å, resulting in a better visual fit to the Fourier transform of the data and a lowering of the error value (Table 4, fit 4). Using two or more ligands with the short component causes the σ^2 value of that component to become abnormally high for short, strong ligands. First coordination sphere components longer than 2.15 Å could not be fit in the data. As with E280K-PAH^{rest}[ ], carbon single- and multiple-scattering components complete the EXAFS fit to E280K-PAH^{act}[L-Phe, 5-deaza-6-MPH$_4$]. Thus, E280K-PAH^{act}[L-Phe, 5-deaza-6-MPH$_4$] is a 6C site similar to E280K-PAH^{rest}[ ]. This is in direct contrast to the behavior of R158Q and WT PAH, each of which converts to a 5C geometry upon binding of cosubstrates. The E280K mutation must therefore perturb the binding of substrate and/or cofactor in the binding pocket, disrupting the mechanism by which water is lost from the active site of WT PAH.

4. Discussion

The catalytic reaction of PAH requires that all three reaction components—L-Phe, pterin, and O_2—be present before any product is released.[17,26,27] Our previous studies on WT PAH have demonstrated that formation of the ternary complex PAH^R[L-Phe, 5-deaza-6-MPH$_4$] results in a 5C site with an open coordination position available on the Fe^{II} for reaction with O_2.[19,20] Our kinetic and spectroscopic studies of two PKU-inducing mutants of PAH, R158Q and E280K, provide further insight into the molecular mechanism of the enzyme. Analysis of the products produced by the mutant enzymes shows that although both oxidize pterin at more than twice the rate of WT enzyme, these reactions are only ∼20% coupled to production of L-Tyr. MCD and XAS studies indicate that the 6C Fe^{II} active site of the resting R158Q-PAH^{rest}[ ] and E280K-PAH^{rest}[ ] species is similar to that of the WT enzyme. When L-Phe and 5-deaza-6-MPH$_4$ are present, however, only R158Q-PAH^{act}[L-Phe, 5-deaza-6-MPH$_4$] loses a ligand to form a 5C site similar to the behavior of the WT enzyme.

The orientations of the substrate and cofactor in the active site of the ternary enzyme complex are configured to minimize nonproductive side reactions, thereby leading to tightly coupled hydroxylation. Analysis of crystal structures of WT PAH[22−25] indicates that both the R158Q and E280K mutations may reorganize the protein matrix in the vicinity of the mutations, affecting binding and orientation of either or both of the pterin and L-Phe cosubstrates. The R158Q mutation is a relatively conservative mutation that will break the hydrogen bond between Arg158 and Glu280. A recent crystal structure of PAH with both BH$_4$ and the L-Phe analogue 3-(2-thienyl)-L-alanine (THA) bound in the active site shows that there is a mobile loop formed by residues 131−155 that refolds in the presence of both BH$_4$ and THA to relocate Tyr138 from the protein surface to the active site.[25] Because Arg158 is adjacent to that loop, it is possible that the loss of the Arg158-Glu280 hydrogen bonding interaction will interfere with correct pterin and/or L-Phe orientation. Arg158 is also near residues 247−251, which provide hydrogen bonds to the pterin cofactor.[25] In contrast, the E280K mutation would have a much more pronounced structural effect on the protein structure because Lys is positively charged and is significantly longer than the negatively charged Glu. The position of Arg158 would likely be disturbed as well as the region around Glu280. Glu280 is part of a Thr278-Pro279-Glu280-Pro218 loop that appears to be adjacent to the substrate-binding pocket;[25] indeed, Thr278 forms a hydrogen-bonding interaction with THA.

These structural interactions correlate with the changes observed for the Fe^{II} site of the mutants, in which binding of both pterin and L-Phe produces a 5C site in R158Q but not in E280K PAH. If the pterin binding pocket is altered by the R158Q mutation so that the pterin is misaligned but L-Phe binding is not significantly perturbed, then the site should behave similarly to that of the WT enzyme. If there is further perturbation to the orientation of pterin and/or L-Phe, as predicted for the E280K mutation, then it is reasonable that the

Scheme 1

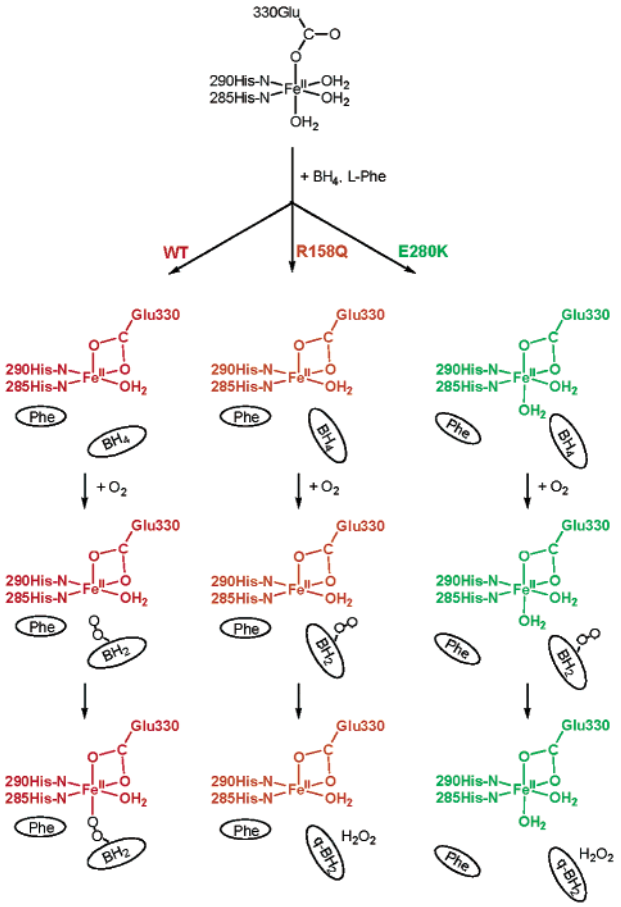

Fe^{II} site would stay 6C as in the resting enzyme. It is important to emphasize that both cosubstrates are still tightly bound to the active site,[34] thus only their orientations and effects on the Fe^{II} ligation may be affected by the mutations.

The overall structural and kinetic effects produced by the R158Q and E280K mutations are consistent with a catalytic mechanism in which pterin reacts with O_2 before interacting with the Fe^{II} site, as depicted in Scheme 1. ^{18}O kinetic isotope effects had demonstrated that a change in oxygen bond order occurs in the first irreversible step for TyrH but could not definitively distinguish whether O_2 was initially reacting with PH_4 or Fe^{II}.[64] Because an open coordination position would facilitate the reaction of O_2 with Fe^{II} and both mutants exhibit essentially equivalent reactivity toward pterin regardless of whether there is an open coordination position on the Fe^{II}, the first step in the mechanism must be reaction of pterin with O_2 to form a peroxy-pterin species. When the pterin is oriented correctly in the active site pocket, as depicted for WT enzyme (red pathway), the next step would be reaction of the peroxy-pterin with 5C Fe^{II} to form the putative Fe^{II}−OO-pterin intermediate. This intermediate would heterolytically cleave to form Fe^{IV}═O and the 4a-OH-pterin product; Fe^{IV}═O would then react with L-Phe to produce L-Tyr and regenerate the Fe^{II} site.

When the pterin is misaligned in the active site pocket, as predicted for R158Q and E280K (Scheme 1, orange and green pathways), the peroxy-pterin species cannot react with the Fe^{II} and decomposes into the quinonoid pterin and H_2O_2. Some flexibility of the active site pocket allowing for different orientations of the pterin (and/or L-Phe) would account for the 20% coupled hydroxylation observed for the two mutants. The apparent increase in pterin oxidation seen in R158Q and E280K relative to WT coupled hydroxylation indicates that reaction of pterin + O_2 proceeds quickly, with the major reaction pathway reminiscent of WT tetrahydropterin oxidase activity. Studies on TyrH have indicated that substrate C−H bond cleavage and product release are not rate limiting,[65,66] suggesting that the rate-determining step in coupled hydroxylation may be heterolytic cleavage of the Fe^{II}−OO-pterin intermediate.

Our investigation into two PKU-inducing mutants of PAH, R158Q and E280K, has provided insight into the reaction and disease mechanisms at a molecular level. The first step of the mechanism is reaction of pterin + O_2 to form a peroxy-pterin species, which then reacts with Fe^{II} if an open coordination position is available on the iron. Because a 5C Fe^{II} species is only present when both pterin and L-Phe are bound to the active site of WT and R158Q PAH, it is likely that the pterin is misaligned in the R158Q enzyme while either or both of pterin and L-Phe may have perturbed orientations in E280K. This raises the possibility of treatment of patients with the R158Q mutation using pterin derivatives, which might improve orientation in the perturbed active site. Such an approach would be more challenging for patients with the E280K mutation as the Fe^{II} active site remains 6C when both L-Phe and pterin are bound, thus it likely cannot participate in heterolytic cleavage of the peroxy-pterin O−O bond.

Acknowledgment. This work was supported by grants from the National Institutes of Health: GM40392 to E.I.S., RR-01209 to K.O.H., GM61208 to J.P.C., and a Stanford-NIH Biotechnology Training Fellowship to J.N.K. SSRL operations are funded by the U.S. Department of Energy (Office of Basic Energy Science). The Structural Molecular Biology program at SSRL is funded by the National Institutes of Health, National Center for Research Resources, Biomedical Technology Program, and the Department of Energy (Office of Biological and Environmental Research).

Note Added in Proof: The coordinates were released in the PDB for the 2.5-Å crystal structure of truncated WT PAH with pterin and Phe analogue (ref 25). It should be noted that the hydrogen-bonding interaction of Arg158 and Glu280 appeared to be altered in this fully-loaded enzyme.

Supporting Information Available: CD spectra for R158Q PAH samples and Gaussian fits for R158Q and E280K PAH MCD data. This material is available free of charge via the Internet at http://pubs.acs.org.

JA029106F

(64) Francisco, W. A.; Tian, G.; Fitzpatrick, P. F.; Klinman, J. P. *J. Am. Chem. Soc.* **1998**, *120*, 4057−4062.
(65) Fitzpatrick, P. F. *Biochemistry* **1991**, *30*, 3658−3662.
(66) Fitzpatrick, P. F. *Biochemistry* **1991**, *30*, 6386−6391.